analytical chemistry

Article

pubs.acs.org/ac

Electrospray Ionization Ion Mobility Mass Spectrometry of Human Brain Gangliosides

Mirela Sarbu,[†,‡] Adrian C. Robu,[‡,§] Roxana M. Ghiulai,[∥] Željka Vukelić,[⊥] David E. Clemmer,[#] and Alina D. Zamfir*[,†,‡]

[†]Aurel Vlaicu University of Arad, 310130 Arad, Romania

[‡]National Institute for Research and Development in Electrochemistry and Condensed Matter, 300569 Timisoara, Romania

[§]West University of Timisoara, 300223 Timisoara, Romania

[∥]Department of Pharmacy, Victor Babes University of Medicine and Pharmacy, 300041 Timisoara, Romania

[⊥]Department of Chemistry and Biochemistry, University of Zagreb Medical School, HR−10000 Zagreb, Croatia

[#]Department of Chemistry, Indiana University, Bloomington, Indiana 47405, United States

ABSTRACT: The progress of ion mobility spectrometry (IMS), together with its association to mass spectrometry (MS), opened new directions for the identification of various metabolites in complex biological matrices. However, glycolipidomics of the human brain by IMS MS represents an area untouched up to now, because of the difficulties encountered in brain sampling, analyte extraction, and IMS MS method optimization. In this study, IMS MS was introduced in human brain ganglioside (GG) research. The efficiency of the method in clinical glycolipidomics was demonstrated on a highly complex mixture extracted from a normal fetal frontal lobe (FL37). Using this approach, a remarkably rich molecular ion pattern was discovered, which proved the presence of a large number of glycoforms and an unpredicted diversity of the ceramide chains. Moreover, the results showed for the first time the occurrence of GGs in the human brain with a much higher degree of sialylation than previously reported. Using IMS MS, the entire series starting from mono- up to octasialylated GGs was detected in FL37. These findings substantiate early clinical reports on the direct correlation between GG sialylation degree and brain developmental stage. Using IMS CID MS/MS, applied here for the first time to gangliosides, a novel, tetrasialylated *O*-GalNAc modified species with a potential biomarker role in brain development was structurally characterized. Under variable collision energy, a high number of sequence ions was generated for the investigated GalNAc−GQ1(d18:1/18:0) species. Several fragment ions documented the presence of the tetrasialo element attached to the inner Gal, indicating that GalNAc−GQ1(d18:1/18:0) belongs to the *d* series.

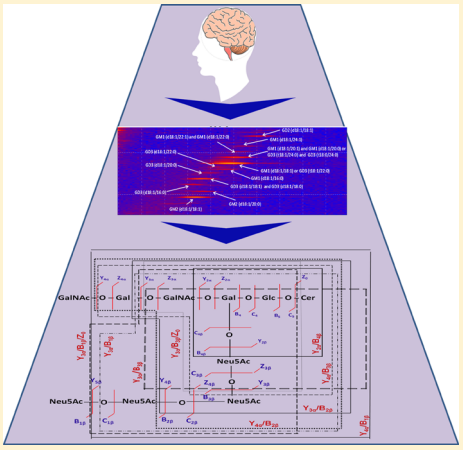

With an extremely fast evolution during the last 30 years, mass spectrometry (MS) represents nowadays one of the most powerful, accurate, and sensitive methods for biomolecule analysis. Highly complex biological mixtures may be characterized by MS in order to achieve significant compositional and structural data that serve for biomarker identification. In these cases, different separation techniques, such as electrophoresis or chromatography, are usually applied prior to MS analysis.[1] As an alternative to these methods, ion mobility separation (IMS) coupled to mass spectrometry has emerged as a robust and reliable analytical system. IMS MS provides a new dimension in the analysis of biomolecules, since, based on the properties of transport driven by the electric field,[2−4] IMS separates the ions according to the differences not only in size but also in the analyte apparent surface area (collision cross section).[5,6] Thus, ion mobility mass spectrometry opened up new directions for detailed structural analysis of biomarkers, since it is able to separate isomers, isobars, and conformers, to reduce the chemical noise, as well as to provide information on the stoichiometry, topology, and cross section of these biological structures with a diagnostic role.[6,7] Besides, structurally similar ions and ions of the same charge state can be separated by IMS into families, which appear along a unique mass−mobility correlation line. The connection between two separation dimensions (e.g., IMS and MS) is manifested as a "trend line", which potentially permits the discrimination of different classes.[2,8,9] Based on all these characteristics, IMS MS alone or in combination with various fragmentation techniques constitutes a unique platform capable of complex mixture separation, detection by MS and structural characterization of a single, often low abundance, compound.

Although it has been extensively applied in the analysis of peptides,[10] proteins,[11] lipids,[12−15] carbohydrates,[16−19] and small

Received: January 13, 2016
Accepted: April 18, 2016
Published: April 18, 2016

DOI: 10.1021/acs.analchem.6b00155
Anal. Chem. 2016, 88, 5166−5178

molecules,[20] IMS MS has played a very limited role in glycolipid research.

Glycosphingolipids (GSL) represent a class of glycolipids in which the hydrophobic lipid moiety represented by a sphingoid or a ceramide is connected through a glycosidic linkage to one or more carbohydrate residues.

Among all GSLs, gangliosides (GGs) have received a particular attention ever since their discovery, 7 decades ago.[21] GGs contain a mono- to polysialylated oligosaccharide chain of variable length attached to a ceramide, which can exhibit different patterns of sphingoid base and fatty acid residues. Although they are ubiquitously found in tissues and body fluids, the particular interest in gangliosides is due to the fact that these biomolecules were identified as highly expressed in central nervous system (CNS), in particular in various brain regions.[22−24] Gangliosides are not just involved in specific biological functions of the brain,[23,24] such as development, maturation, and aging, but are also correlated to certain diseases, such as hereditary disorders,[21] malignant transformations,[25] Guillain−Barré syndrome,[26,27] GM1 gangliosidosis (Tay−Sachs disease),[28,29] GM2 gangliosidosis (Sandhoff disease),[28,29] and so on, through aberrant glycosylation pathways. Moreover, the onset of Alzheimer's disease, the most common form of dementia and neurodegenerative disease, is related to the aggregation of amyloid-β peptide by gangliosides.[30]

Due to the high diversity and structural complexity of GGs, until recently, the studies focused on composition determination and quantification were performed exclusively by chromatography, immunochemical, and immunohistochemical techniques;[31,32] nevertheless, the data generated by these methods were based primarily on comparison and, moreover, allowed only major ganglioside species detection. Nowadays, the achievement of precise structural analysis of gangliosides does not constitute an impediment to identify and characterize the detailed structure of all species, not just of those highly expressed. This is now possible due to the unmatched characteristics of mass spectrometry, the main analytical tool for the investigation of such molecules.

Since 2001, structural elucidation of gangliosides extracted from fetal and adult brain regions at different gestational stages in health or disease are investigated by advanced MS in order to determine their specific composition and to correlate this specificity with the specialized function of each area of the CNS. The studies were conducted using platforms based either on quadrupole time-of-flight (QTOF), Fourier transform ion cyclotron resonance (FTICR) or high capacity ion trap (HCT) mass spectrometers. Hence, fetal cerebellum,[33] occipital and frontal lobes,[34] fetal frontal neocortex,[34] fetal hippocampus,[35] anencephalic residual brain tissue,[36] and brain tumors[37−39] were thoroughly characterized with respect to their ganglioside profile. Also, the native ganglioside mixtures extracted from normal fetal frontal lobe in different developmental stages were analyzed by fully automated chip-based nanoelectrospray (nanoESI) ion trap MS and multistage MS. All the studies performed up to now allowed the detection and structural characterization of individual species in complex native mixtures, enabling the correlation of GG expression and specificity with a certain pathological state and ultimately, disease biomarker discovery.

So far, GGs were approached by IMS only in conjunction with MALDI TOF MS in a study performed in positive ion mode by Jackson et al.[40] Using addition of cesium to the matrix to enhance positive ionization, the authors investigated commercially available GD1a and GD1b fractions and a ganglioside extract from mouse cerebrum. The generated results demonstrated that the separation of gangliosides is according to the number of sialic acids and the mobility drift time increases with the number of sialic acid residues.[40] Nevertheless, for ganglioside analysis, IMS MS was never developed: (i) in combination with ESI; (ii) in the negative ion mode; (iii) in combination with fragmentation analysis by tandem MS (MS/MS); (iv) for native extracts of human origin.

In this context, in the current study, for the first time, ESI IMS MS and MS/MS was optimized in negative ion mode and introduced in the study of GGs extracted from human brain. The efficiency of the method in clinical glycolipidomics was demonstrated on a highly complex native mixture extracted and purified from a normal fetal frontal lobe in the 37th gestational week (gw) (FL37). By this approach, a remarkably rich molecular ion pattern, and a high diversity of the ceramide chain for certain species, was observed. For the first time, GGs of a much higher degree of sialylation were identified in the human brain. The ionization and the detection of the low-abundance species, such as the polysialylated GGs, was possible due to the ion mobility separation that allowed the differentiation of gangliosides based on the carbohydrate chain length and the degree of sialylation through the formation of "trend lines". The combination of IMS with MS/MS by collision-induced dissociation (CID), applied here for the first time to gangliosides, confirmed the structure of a newly identified GalNAc−GQ1 (d18:1/18:0) species belonging to the *d* ganglioside series.

The information collected by IMS MS substantiates previous hypotheses on the direct correlation between ganglioside sialylation degree and brain developmental stage.[4,36,41]

MATERIALS AND METHODS

Reagents and Materials. Analytical-grade methanol used without further purification for sample preparation was purchased from Sigma (St. Louis, MO, U.S.A.). All sample solutions were dried in a SpeedVac Concentrator, SPD 111 V-230 from Thermo Electron Corporation (Ashville, NC, U.S.A.), coupled to a vacuum pump, PC 2002 Vario with CVC 2000 Controller from Vaccubrand (Wertheim, Germany).

Frontal Lobe Sampling. The native ganglioside mixture analyzed in this study was purified from a normal fetal frontal lobe, FL37. Brain sample analyzed in the present study was obtained during routine pedopathological section/autopsy examination at Clinical Hospital for Obstetrics and Gynecology "Petrova" and Department of Forensic Medicine and Criminology, Faculty of Medicine, University of Zagreb, Croatia. The age of the fetus was deduced from (i) the mother's menstrual history; (ii) the echographic fetal biometry conducted during pregnancy follow-up; (iii) specific measurements of the aborted fetuses, such as the femoral length, the biparietal perimeter and the humerus length together with weight measurements. The fetus deceased because of spontaneous abortion. During pedopathological examination, including histopathological analysis of the tissue, no signs of malformation, aberrant development, or brain affliction were found.[42] Therefore, the brain was considered as normal for the given gestational stage. After sampling, the frontal lobe was weighed and stored at −20 °C until the ganglioside extraction procedure.

Gangliosides Extraction and Purification. The extraction and purification of FL37 GGs mixture followed the procedures described before[43,44] and the method developed by Svennerholm and Fredman[45] as modified by Vukelić et al.[22] The first step in

DOI: 10.1021/acs.analchem.6b00155
Anal. Chem. 2016, 88, 5166−5178

GGs extraction consisted in homogenizing the tissue in ice-cold water. Lipids extraction was performed twice using a chloroform−methanol−water mixture (1:2:0.75, by volume). In order to separate GGs from other lipids, a phase partition followed by repartition was carried out by adding to the combined supernatant resulted after centrifugation chloroform, methanol, and water up to a final volume ratio of 1:1:0.8. The combined upper phases containing polar glycosphingolipids (gangliosides) were collected. The crude GG extract was purified in several steps as described by us previously.[42] Permission for experiments with human tissue for scientific purposes was obtained from the Ethical Commission of the Zagreb Medical Faculty under project 108120 financed by the Croatian Ministry of Science and Technology.

For IMS MS analysis, a stock solution of the native GG extract (~1 mg/mL) was prepared by dissolving the dried material in pure methanol. Dilution of the stock solution in pure methanol yielded the working aliquot concentration of approximately 5 pmol/μL (calculated for an average molecular weight of 2000). Prior to MS analysis, the sample solution was centrifuged for 1 h at 6000 rpm in a mini-centrifuge (Thermo Fisher Scientific, U.S.A.). The supernatant was collected and submitted to (−) ESI IMS MS and MS/MS analysis by CID at low energies.

Ion Mobility Mass Spectrometry. All ion mobility mass spectrometry experiments were conducted on a Synapt G2s mass spectrometer (Waters, Manchester, U.K.) equipped with ESI source. The ganglioside sample was infused by syringe pump at a 2 μL/min flow rate.

All mass spectra (MS and MS/MS) were acquired in the negative ion mode, within the mass range 100−3000 m/z, with a speed of 1 scan/s. For all experiments, the capillary potential was maintained at 2 kV, a value that proved to generate an efficient ionization of the components. The desolvation gas was adjusted to 100 L/h, while the desolvation temperature was set to 350 °C and kept at this value during all experiments. Other parameters were set as follows: the cone voltage was kept at 40 V, while the source block temperature at 100 °C. Low-mass (LM) and high-mass (HM) resolution parameters were set at 12 and 15, respectively, for the MS experiments, while for MS/MS experiments they were adjusted at 10 and 15, respectively.

The opening of the shutter grid allowed the release of a packet of ions that passed through the quadrupole and reached the T-wave region. As the ions migrated through the drift region under an electric field, structures with different charges, masses and/or conformations were separated according to differences in their mobility through the buffer gas. To enhance the separation, the IMS parameters were thoroughly optimized as follows: wave velocity at 650 m/s, IMS wave height at 40 V, and IMS gas flow at 90 L/min. These values provided the best separation not only for the molecular ions in the mixture screened in the MS mode but also for the mass-selected ions in the quadrupole submitted further to CID MS/MS. The T-wave mobility cell contained nitrogen. After separation in the drift tube, the ions were extracted into a TOF source for mass analysis. The TOF analyzer was operated in the V-mode with an average mass resolution of 20 000.

The fragmentation by CID was performed after mobility separation in the transfer cell and not in the trap section, because in the transfer cell, the discrimination of the parent ion isomers is provided. By using this approach, we were able to observe the potential isomers for the chosen precursor ions. In order to generate the maximum number of diagnostic ions, energies between 10 and 45 eV were employed. Data acquisition and processing were performed using MassLynx (version V4.1, SCN 855) and Waters Driftscope (version V2.7). The system introduced by Svennerholm[46] and the recommendations of IUPAC-IUB Commission on Biochemical Nomenclature (IUPAC-IUB 1998)[47] were followed for abbreviations of gangliosides and the precursor glycosphingolipids. The carbohydrate sequence ions were assigned on the basis of the nomenclature introduced by Domon and Costello.[48] All the signals in the spectra were assigned to specific ions by comparing the experimental m/z with the calculated theoretical values.

RESULTS AND DISCUSSION

IMS MS Analysis. Thirty microliters of FL37 sample solution at 5 pmol/μL concentration extracted and purified from frontal lobe tissue were loaded into the syringe and submitted to negative ion mode ESI IMS MS. After ionization, a packet of ions was introduced into the drift tube containing the buffer gas; here, the ions migrated through the gas under the influence of a mild electric field and individual GGs in the mixture were separated due to differences in their mobility through the gas.

The two-dimensional data set of FL37, generated after 6 min of signal acquisition is presented in Figure 1, together with the resulted total ion chromatogram (TIC) and the full spectrum.

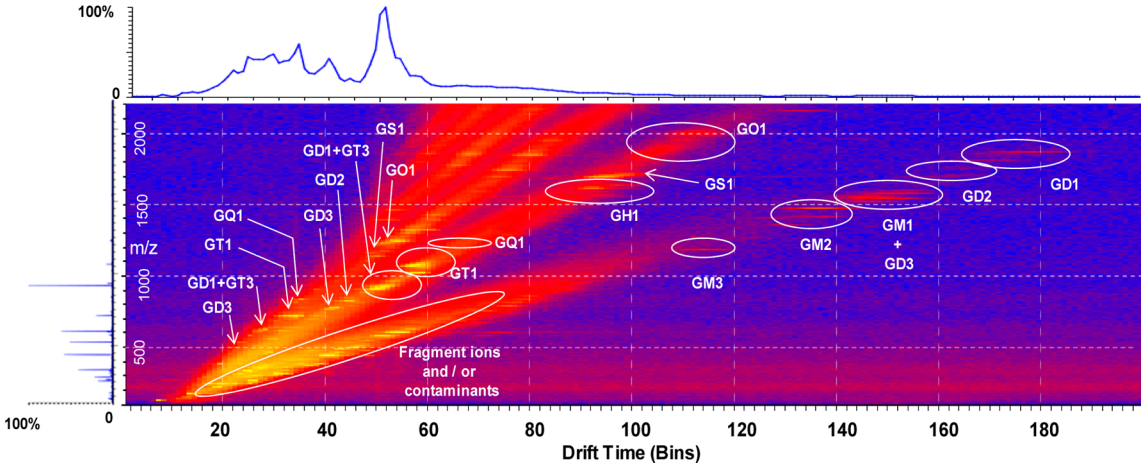

Figure 1. Driftscope display of the negative ions from FL 37 sample. The m/z vs drift time plot reveals the separation of the gangliosides based on the carbohydrate chain length and the degree of sialylation.

DOI: 10.1021/acs.analchem.6b00155
Anal. Chem. 2016, 88, 5166−5178

Table 1. Assignment of Major Ionic Species Detected in the FL37 Mixture by IMS MS[a]

no. crt.	*m/z* experimental	*m/z* theoretical	mass accuracy (ppm)	proposed structure	molecular ion
1	477.608	477.611	6.289	GM2 (d18:1/22:2)	$[M-3H^+]^{3-}$
2	498.274	498.277	6.024	GD3 (d18:1/20:1)	$[M-3H^+]^{3-}$
3	502.293	502.289	7.968	GD3 (d18:1/22:0)	$[M-H_2O-3H^+]^{3-}$
4	526.301	526.297	7.605	GM1 (d18:1/22:1)	$[M-H_2O-3H^+]^{3-}$
5	531.014	531.009	9.416	GT1 (d18:1/18:0)	$[M-4H^+]^{4-}$
6	545.029	545.025	7.339	GT1 (d18:1/22:0)	$[M-4H^+]^{4-}$
7	546.971	546.975	7.326	*O*−Ac−GM1 (d18:1/22:0)	$[M-3H^+]^{3-}$
8	551.021	551.025	7.260	GT1 (d18:1/24:2)	$[M-4H^+]^{4-}$
9	555.027	555.023	7.207	GT1 (t18:1/24:2)	$[M-4H^+]^{4-}$
10	559.291	559.295	7.156	GD2 (d18:1/20:2)	$[M-H_2O-3H^+]^{3-}$
11	563.949	563.954	8.881	GD2 (d18:1/18:1)	$[M-H_2O-4H^+ +Na^+]^{3-}$
12	574.974	574.982	13.937	Fuc−GM1 (d18:1/22:1)	$[M-H_2O-3H^+]^{3-}$
13	586.635	586.637	3.413	GT3 (t18:0/18:0)	$[M-H_2O-3H^+]^{3-}$
14	595.972	595.981	15.126	GT3 (t18:0/20:0)	$[M-H_2O-3H^+]^{3-}$
15	596.770	596.775	8.389	GQ1 (d18:1/16:0)	$[M-4H^+]^{4-}$
16	600.637	600.641	6.667	GT3 (t18:1/20:1)	$[M-3H^+]^{3-}$
17	603.778	603.783	8.292	GQ1 (d18:1/18:0)	$[M-4H^+]^{4-}$
18	610.784	610.791	11.475	GQ1 (d18:1/20:0)	$[M-4H^+]^{4-}$
19	611.310	611.316	9.819	GD1 (d18:1/18:0)	$[M-3H^+]^{3-}$
20	613.987	613.997	16.313	GT3 (d18:1/24:1)	$[M-3H^+]^{3-}$
21	613.805	613.800	8.157	GQ1 (d18:0/22:0)	$[M-H_2O-4H^+]^{4-}$
22	617.793	617.799	9.724	GQ1 (d18:1/22:0)	$[M-4H^+]^{4-}$
23	621.327	621.332	8.052	GD1 (d18:0/20:0)	$[M-3H^+]^{3-}$
24	624.296	624.302	9.615	GQ1 (d18:1/24:1)	$[M-4H^+]^{4-}$
25	637.960	637.967	10.989	Fuc−GT3 (t18:1/16:1)	$[M-4H^+ +Na^+]^{3-}$
26	644.383	644.388	7.764	GM3 (d18:1/24:0)	$[M-H_2O-4H^+ +2Na^+]^{2-}$
27	674.867	674.873	8.902	GM2 (d18:1/16:2)	$[M-2H^+]^{2-}$
28	676.551	676.557	8.876	GP1 (d18:1/18:0)	$[M-4H^+]^{4-}$
29	683.65	683.657	10.249	GT1 (d18:1/14:0)	$[M-H_2O-3H^+]^{3-}$
30	689.649	689.660	15.965	GT1 (d18:1/14:0)	$[M-3H^+]^{3-}$
31	698.998	699.004	8.584	GT1 (d18:1/16:0)	$[M-3H^+]^{3-}$
32	707.668	707.676	11.315	GT1 (d18:1/18:1)	$[M-3H^+]^{3-}$
33	707.921	707.914	9.901	GM2 (d18:1/22:2)	$[M-H_2O-2H^+]^{2-}$
34	708.338	708.348	14.124	GT1 (d18:1/18:0)	$[M-3H^+]^{3-}$
35	713.002	713.008	8.415	GT1 (t18:1/18:1)	$[M-3H^+]^{3-}$
36	713.666	713.659	9.818	GT1 (d18:1/16:0)	$[M-5H^+ +2Na^+]^{3-}$
37	714.339	714.351	16.806	GT1 (t18:0/18:0)	$[M-3H^+]^{3-}$
38	717.013	717.020	9.763	GT1 (d18:1/20:1)	$[M-3H^+]^{3-}$
39	717.681	717.692	15.342	GT1 (d18:1/20:0)	$[M-3H^+]^{3-}$
40	716.927	716.920	9.777	GM2 (d18:1/22:2)	$[M-2H^+]^{2-}$
41	720.889	720.896	9.722	GD3 (d18:1/16:0)	$[M-2H^+]^{2-}$
42	722.345	722.352	9.695	GT1 (t18:1/20:1)	$[M-3H^+]^{3-}$
43	726.359	726.363	6.887	GT1 (d18:1/22:1)	$[M-3H^+]^{3-}$
44	727.023	727.036	17.881	GT1 (d18:1/22:0)	$[M-3H^+]^{3-}$
45	731.688	731.695	9.576	GT1 (t18:1/22:1)	$[M-3H^+]^{3-}$
46	733.893	733.904	15.007	GD3 (d18:1/18:1)	$[M-2H^+]^{2-}$
47	734.905	734.912	9.537	GD3 (d18:1/18:0)	$[M-2H^+]^{2-}$
48	735.026	735.035	12.244	*O*−Ac−GT1 (d18:1/22:0)	$[M-H_2O-3H^+]^{3-}$
49	735.699	735.707	10.884	*O*−Ac−GT1 (d18:0/22:0)	$[M-H_2O-3H^+]^{3-}$
50	748.921	748.928	9.358	GD3 (d18:1/20:0)	$[M-2H^+]^{2-}$
51	762.937	762.943	7.874	GD3 (d18:1/22:0)	$[M-2H^+]^{2-}$
52	771.942	771.949	9.079	GD3 (t18:0/22:0)	$[M-2H^+]^{2-}$
53	775.730	775.722	10.323	Fuc−GT1 (d18:1/22:0)	$[M-3H^+]^{3-}$
54	775.944	775.951	9.032	GD3 (d18:1/24:1)	$[M-2H^+]^{2-}$
55	781.717	781.725	10.243	Fuc−GT1 (t18:0/22:0)	$[M-3H^+]^{3-}$
56	794.013	794.020	8.816	GQ1 (d18:1/16:3)	$[M-3H^+]^{3-}$
57	796.029	796.036	8.794	GQ1 (d18:1/16:0)	$[M-3H^+]^{3-}$
58	804.695	804.708	16.169	GQ1 (d18:1/18:1)	$[M-3H^+]^{3-}$
59	806.943	806.951	9.926	*O*−Ac GM1 (d18:1/20:0)	$[M-2H^+]^{2-}$
60	811.941	811.949	9.864	GD3 (d18:1/26:1)	$[M-4H^+ +2Na^+]^{2-}$
61	812.699	812.707	9.852	GQ1 (d18:1/18:0)	$[M-4H^+ +Na^+]^{3-}$

DOI: 10.1021/acs.analchem.6b00155
Anal. Chem. 2016, 88, 5166−5178

Table 1. continued

no. crt.	*m/z* experimental	*m/z* theoretical	mass accuracy (ppm)	proposed structure	molecular ion
62	814.716	814.724	9.828	GQ1 (d18:1/20:0)	$[M-3H^+]^{3-}$
63	819.373	819.383	12.210	*O*−Ac−GQ1 (d18:1/18:0)	$[M-3H^+]^{3-}$
64	824.035	824.043	9.709	*O*−Ac−GQ1 (t18:1/18:1)	$[M-3H^+]^{3-}$
65	832.731	832.739	9.615	GQ1 (t18:1/24:0)	$[M-H_2O-3H^+]^{3-}$
66	835.435	835.444	10.778	GD2 (d18:1/18:1)	$[M-2H^+]^{2-}$
67	836.445	836.452	8.373	GD2 (d18:1/18:0)	$[M-2H^+]^{2-}$
68	850.459	850.467	9.412	GD2 (d18:1/20:0)	$[M-2H^+]^{2-}$
69	889.456	889.465	10.124	GT3 (t18:0/18:0)	$[M-2H^+]^{2-}$
70	894.466	894.475	10.067	GT3 (t18:0/20:0)	$[M-H_2O-2H^+]^{2-}$
71	902.403	902.412	9.978	GP1 (d18:1/18:0)	$[M-3H^+]^{3-}$
72	903.472	903.462	11.074	GD1 (d18:1/16:0)	$[M-2H^+]^{2-}$
		903.481	9.967	GT3 (t18:0/20:0)	$[M-2H^+]^{2-}$
73	908.463	908.473	11.013	GD1 (d18:1/18:0)	$[M-H_2O-2H^+]^{2-}$
74	916.461	916.470	9.825	GD1 (d18:1/18:1)	$[M-2H^+]^{2-}$
75	917.468	917.478	10.905	GD1 (d18:1/18:0)	$[M-2H^+]^{2-}$
76	923.509	923.515	6.501	GT3 (d18:0/24:0)	$[M-2H^+]^{2-}$
77	930.465	930.486	22.580	GD1 (d18:1/20:1)	$[M-2H^+]^{2-}$
		930.474	9.677	*O*−Ac GT3 (d18:1/22:1)	$[M-H_2O-3H^+ +Na^+]^{2-}$
78	931.475	931.494	20.408	GD1 (d18:1/20:0)	$[M-2H^+]^{2-}$
		931.482	7.518	*O*−Ac GT3 (d18:1/22:0)	$[M-H_2O-3H^+ +Na^+]^{2-}$
79	944.481	944.501	21.186	GD1 (d18:1/22:1)	$[M-2H^+]^{2-}$
		944.490	9.534	*O*−Ac GT3 (d18:1/24:1)	$[M-H_2O-3H^+ +Na^+]^{2-}$
80	945.488	945.510	23.280	GD1 (d18:1/22:0)	$[M-2H^+]^{2-}$
		945.498	10.582	*O*−Ac GT3 (d18:1/24:0)	$[M-H_2O-3H^+ +Na^+]^{2-}$
81	951.481	951.491	10.515	*O*−Ac GD1 (d18:1/20:1)	$[M-2H^+]^{2-}$
82	952.489	952.499	10.504	*O*−Ac GD1 (d18:1/20:0)	$[M-2H^+]^{2-}$
83	957.446	957.454	8.359	Fuc−GT3 (t18:1/16:1)	$[M-3H^+ +Na^+]^{2-}$
84	958.453	958.462	9.395	Fuc−GT3 (t18:1/16:0)	$[M-3H^+ +Na^+]^{3-}$
85	966.507	966.497	10.351	Fuc−GT3 (d18:1/20:1)	$[M-2H^+]^{2-}$
		966.514	7.246	*O*−Ac GD1 (d18:1/22:0)	$[M-2H^+]^{2-}$
86	967.512	967.504	8.273	Fuc−GT3 (d18:1/20:0)	$[M-2H^+]^{2-}$
		967.522	10.341	*O*−Ac GD1 (d18:0/22:0)	$[M-2H^+]^{2-}$
87	972.464	972.477	13.374	Fuc−GT3 (t18:1/18:0)	$[M-2H^+]^{2-}$
88	980.502	980.512	10.204	Fuc−GT3 (d18:1/22:1)	$[M-2H^+]^{2-}$
89	988.482	988.492	10.121	Fuc−GD1 (d18:1/18:2)	$[M-2H^+]^{2-}$
90	989.489	989.499	10.111	Fuc−GD1 (d18:1/18:1)	$[M-2H^+]^{2-}$
91	990.497	990.507	10.101	Fuc−GD1 (d18:1/18:0)	$[M-2H^+]^{2-}$
92	991.503	991.515	12.109	Fuc−GD1 (d18:0/18:0)	$[M-2H^+]^{2-}$
93	992.502	992.512	10.081	Fuc−GT3 (d18:1/24:3)	$[M-2H^+]^{2-}$
94	1017.941	1017.955	13.675	GT1 (d18:1/12:3)	$[M-2H^+]^{2-}$
95	1018.952	1018.963	10.806	GT1 (d18:1/12:2)	$[M-2H^+]^{2-}$
96	1027.958	1027.969	10.711	GT1 (t18:1/12:1)	$[M-2H^+]^{2-}$
97	1032.969	1032.979	9.689	GT1 (d18:1/14:2)	$[M-2H^+]^{2-}$
98	1038.948	1038.960	11.561	GT1 (t18:1/12:1)	$[M-3H^+ +Na^+]^{2-}$
99	1044.967	1044.978	10.536	GT1 (d18:1/14:1)	$[M-3H^+ +Na^+]^{2-}$
100	1048.998	1049.010	11.439	GT1 (d18:1/16:0)	$[M-2H^+]^{2-}$
101	1050.985	1050.996	10.476	GT1 (d18:1/16:0)	$[M-H_2O-3H^+ +Na^+]^{2-}$
102	1059.991	1060.001	9.434	GT1 (d18:1/16:0)	$[M-3H^+ +Na^+]^{2-}$
103	1060.998	1061.010	11.310	GT1 (d18:1/18:2)	$[M-2H^+]^{2-}$
104	1062.009	1062.018	8.475	GT1 (d18:1/18:1)	$[M-2H^+]^{2-}$
105	1063.015	1063.026	10.348	GT1 (d18:1/18:0)	$[M-2H^+]^{2-}$
106	1074.007	1074.018	10.242	GT1 (d18:1/20:3)	$[M-2H^+]^{2-}$
		1074.017	9.310	GT1 (d18:1/18:0)	$[M-3H^+ +Na^+]^{2-}$
107	1077.031	1077.042	10.214	GT1 (d18:1/20:0)	$[M-2H^+]^{2-}$
108	1084.018	1084.031	11.993	GT1 (t18:1/20:1)	$[M-2H^+]^{2-}$
109	1088.022	1088.034	11.029	GT1 (d18:1/22:3)	$[M-2H^+]^{2-}$
110	1091.043	1091.057	12.832	GT1 (d18:1/22:0)	$[M-2H^+]^{2-}$
111	1100.051	1100.063	10.909	GT1 (t18:0/22:0)	$[M-2H^+]^{2-}$
112	1104.051	1104.065	12.681	GT1 (d18:1/24:1)	$[M-2H^+]^{2-}$
113	1115.042	1115.056	12.556	GT1 (d18:1/24:1)	$[M-3H^+ +Na^+]^{2-}$
114	1125.813	1125.805	7.111	GS1 (t18:1/20:0)	$[M-5H^+ +2Na^+]^{3-}$

DOI: 10.1021/acs.analchem.6b00155
Anal. Chem. 2016, 88, 5166−5178

Table 1. continued

no. crt.	*m/z* experimental	*m/z* theoretical	mass accuracy (ppm)	proposed structure	molecular ion
115	1126.472	1126.477	4.440	GS1 (t18:0/20:0)	$[M-5H^+ +2Na^+]^{3-}$
116	1135.151	1135.149	1.762	GS1 (t18:1/22:0)	$[M-5H^+ +2Na^+]^{3-}$
117	1135.828	1135.821	6.167	GS1 (t18:0/22:0)	$[M-5H^+ +2Na^+]^{3-}$
118	1165.081	1165.094	11.159	Fuc−GT1 (d18:0/22:0)	$[M-2H^+]^{2-}$
119	1169.497	1169.500	2.566	GalNAc−GS1 (t18:1/18:0)	$[M-3H^+]^{3-}$
120	1176.826	1176.827	0.850	GalNAc−GS1 (t18:1/18:0)	$[M-4H^+ +Na^+]^{3-}$
121	1177.726	1177.721	4.24	GM3 (d18:1/18:1)	$[M-H^+]^-$
122	1179.087	1179.110	19.508	Fuc−GT1 (d18:0/24:0)	$[M-2H^+]^{2-}$
123	1179.724	1179.737	11.026	GM3 (d18:1/18:0)	$[M-H^+]^-$
124	1194.162	1194.171	7.538	GalNAc−GS1 (t18:1/22:2)	$[M-4H^+ +Na^+]^{3-}$
125	1207.553	1207.566	10.771	GQ1 (d18:1/18:1)	$[M-2H^+]^{2-}$
126	1208.560	1208.574	11.589	GQ1 (d18:1/18:0)	$[M-2H^+]^{2-}$
127	1214.150	1214.165	12.356	GO1 (t18:0/18:0)	$[M-5H^+ +2Na^+]^{3-}$
128	1218.543	1218.557	11.494	GQ1 (d18:1/18:1)	$[M-3H^+ +Na^+]^{2-}$
129	1219.551	1219.565	11.485	GQ1 (d18:1/18:0)	$[M-3H^+ +Na^+]^{2-}$
130	1222.574	1222.589	12.275	GQ1 (d18:1/20:0)	$[M-2H^+]^{2-}$
131	1222.823	1222.837	11.457	GO1 (t18:1/20:0)	$[M-5H^+ +2Na^+]^{3-}$
132	1229.561	1229.579	14.646	*O*−Ac GQ1 (d18:1/18:0)	$[M-2H^+]^{2-}$
133	1230.149	1230.164	12.195	GO1 (t18:1/20:0)	$[M-6H^+ +3Na^+]^{3-}$
134	1232.837	1232.853	12.987	GO1 (t18:0/22:0)	$[M-5H^+ +2Na^+]^{3-}$
135	1236.579	1236.605	21.036	GQ1 (d18:1/22:0)	$[M-2H^+]^{2-}$
136	1239.494	1239.508	11.299	GO1 (t18:1/22:0)	$[M-6H^+ +3Na^+]^{3-}$
137	1248.844	1248.852	6.410	GO1 (t18:1/24:0)	$[M-6H^+ +3Na^+]^{3-}$
138	1249.598	1249.613	12.009	GQ1 (t18:1/24:0)	$[M-H_2O-2H^+]^{2-}$
139	1310.128	1310.113	11.450	GalNAc−GQ1 (d18:1/18:0)	$[M-2H^+]^{2-}$
140	1321.121	1320.104	12.648	GalNAc−GQ1 (d18:1/18:0)	$[M-3H^+ +Na^+]^{2-}$
141	1350.770	1350.753	12.592	GM2 (d18:1/16:2)	$[M-H^+]^-$
142	1354.768	1354.785	12.555	GM2 (d18:1/16:0)	$[M-H^+]^-$
143	1380.782	1380.800	13.043	GM2 (d18:1/18:1)	$[M-H^+]^-$
144	1382.797	1382.816	13.748	GM2 (d18:1/18:0)	$[M-H^+]^-$
145	1410.826	1410.847	14.894	GM2 (d18:1/20:0)	$[M-H^+]^-$
146	1438.858	1438.879	14.604	GM2 (d18:1/22:0)	$[M-H^+]^-$
147	1440.767	1440.785	12.500	GD3 (d18:1/16:1)	$[M-H^+]^-$
148	1442.783	1442.801	12.482	GD3 (d18:1/16:0)	$[M-H^+]^-$
149	1463.639	1463.658	12.987	GalNAc−GP1 (t18:1/18:0)	$[M-2H^+]^{2-}$
150	1468.820	1468.816	2.724	GD3 (d18:1/18:1)	$[M-H^+]^-$
151	1470.813	1470.832	12.925	GD3 (d18:1/18:0)	$[M-H^+]^-$
152	1498.844	1498.863	12.684	GD3 (d18:1/20:0)	$[M-H^+]^-$
153	1507.646	1507.667	13.935	GH1 (t18:1/18:0)	$[M-2H^+]^{2-}$
154	1516.817	1516.838	13.852	GM1 (d18:1/16:0)	$[M-H^+]^-$
155	1518.636	1518.657	13.834	GH1 (t18:1/18:0)	$[M-3H^+ +Na^+]^{2-}$
156	1526.876	1526.895	12.451	GD3 (d18:1/22:0)	$[M-H^+]^-$
157	1542.869	1542.853	10.376	GM1 (d18:1/18:1)	$[M-H^+]^-$
		1542.890	13.619	GD3 (t18:1/22:0)	$[M-H^+]^-$
158	1543.641	1543.664	14.906	GH1 (t18:1/20:0)	$[M-4H^+ +2Na^+]^{2-}$
159	1544.649	1544.672	14.896	GH1 (t18:0/20:0)	$[M-4H^+ +2Na^+]^{2-}$
160	1544.849	1544.869	12.953	GM1 (d18:1/18:0)	$[M-H^+]^-$
161	1552.884	1552.910	16.753	GD3 (d18:1/24:1)	$[M-H^+]^-$
162	1558.826	1558.848	14.121	*O*−Ac GM1 (d18:1/16:0)	$[M-H^+]^-$
163	1570.901	1570.884	10.828	GM1 (d18:1/20:1)	$[M-H^+]^-$
		1570.921	12.739	GD3 (t18:1/24:0)	$[M-H^+]^-$
164	1572.917	1572.900	10.814	GM1 (d18:1/20:0)	$[M-H^+]^-$
		1572.937	12.723	GD3 (t18:0/24:0)	$[M-H^+]^-$
165	1586.857	1586.879	13.871	*O*−Ac GM1 (d18:1/18:0)	$[M-H^+]^-$
166	1598.893	1598.916	14.393	GM1 (d18:1/22:1)	$[M-H^+]^-$
167	1600.920	1600.931	6.875	GM1 (d18:1/22:0)	$[M-H^+]^-$
168	1609.185	1609.206	13.052	GalNAc−GH1 (t18:1/18:0)	$[M-2H^+]^{2-}$
169	1620.172	1620.197	15.432	GalNAc−GH1 (t18:1/18:0)	$[M-3H^+ +Na^+]^{2-}$
170	1623.198	1623.222	14.787	GalNAc−GH1 (t18:1/20:0)	$[M-2H^+]^{2-}$
171	1624.915	1624.931	9.852	GM1 (d18:1/24:2)	$[M-2H^+]^{2-}$
		1624.905	6.157	GD3 (d18:1/26:1)	$[M-3H^+ +2Na^+]^{2-}$

DOI: 10.1021/acs.analchem.6b00155
Anal. Chem. 2016, 88, 5166−5178

Table 1. continued

no. crt.	*m/z* experimental	*m/z* theoretical	mass accuracy (ppm)	proposed structure	molecular ion
172	1626.929	1626.947	11.070	GM1 (d18:1/24:1)	$[M-2H^+]^{2-}$
		1626.921	4.92	GD3 (d18:1/26:0)	$[M-3H^+ +2Na^+]^{2-}$
173	1640.962	1640.963	0.609	*O*−Ac−GD3 (t18:1/26:0)	$[M-H^+]^-$
174	1671.873	1671.896	13.764	GD2 (d18:1/18:1)	$[M-H^+]^-$
175	1673.878	1673.911	19.725	GD2 (d18:1/18:0)	$[M-H^+]^-$
176	1675.172	1675.196	14.328	GS1 (t18:1/18:0)	$[M-4H^+ +2Na^+]^{2-}$
177	1689.187	1689.212	14.802	GS1 (t18:1/20:0)	$[M-4H^+ +2Na^+]^{2-}$
178	1690.903	1690.927	14.201	Fuc−GM1 (d18:1/18:0)	$[M-H^+]^-$
179	1700.177	1700.203	15.294	GS1 (t18:1/20:0)	$[M-5H^+ +3Na^+]^{2-}$
180	1701.920	1701.943	13.521	GD2 (d18:1/20:0)	$[M-H^+]^-$
181	1714.193	1714.218	14.585	GS1 (t18:1/22:0)	$[M-5H^+ +3Na^+]^{2-}$
182	1754.729	1754.754	14.253	GalNAc−GS1 (t18:1/18:0)	$[M-2H^+]^{2-}$
183	1765.720	1765.745	14.164	GalNAc−GS1 (t18:1/18:0)	$[M-3H^+ +Na^+]^{2-}$
184	1776.708	1776.736	15.766	GalNAc−GS1 (t18:1/18:0)	$[M-4H^+ +2Na^+]^{2-}$
185	1790.727	1790.752	13.966	GalNAc−GS1 (t18:1/20:0)	$[M-4H^+ +2Na^+]^{2-}$
186	1807.896	1807.933	20.476	GD1 (d18:1/16:0)	$[M-H^+]^-$
187	1833.922	1833.949	14.729	GD1 (d18:1/18:1)	$[M-H^+]^-$
188	1834.737	1834.760	12.541	GO1 (t18:1/20:0)	$[M-4H^+ +2Na^+]^{2-}$
189	1835.937	1835.964	14.714	GD1 (d18:1/18:0)	$[M-H^+]^-$
190	1835.739	1835.767	15.259	GO1 (t18:0/20:0)	$[M-4H^+ +2Na^+]^{2-}$
191	1845.725	1845.751	14.092	GO1 (t18:1/20:0)	$[M-5H^+ +3Na^+]^{2-}$
192	1846.729	1846.758	15.709	GO1 (t18:0/20:0)	$[M-5H^+ +3Na^+]^{2-}$
193	1856.714	1856.741	14.547	GO1 (t18:1/20:0)	$[M-6H^+ +4Na^+]^{2-}$
194	1857.721	1857.749	15.078	GO1 (t18:0/20:0)	$[M-6H^+ +4Na^+]^{2-}$
195	1857.919	1857.946	14.539	GD1 (d18:1/18:0)	$[M-2H^+ +Na^+]^-$
196	1860.748	1860.774	13.978	GO1 (t18:0/22:0)	$[M-2H^+ +Na^+]^-$
197	1863.967	1863.996	15.566	GD1 (d18:1/20:0)	$[M-H^+]^-$
198	1871.735	1871.765	16.034	GO1 (t18:0/22:0)	$[M-6H^+ +4Na^+]^{2-}$
199	1877.948	1877.975	14.385	GD1 (t18:1/20:1)	$[M-H^+]^-$
200	1885.752	1885.781	15.384	GO1 (t18:0/24:0)	$[M-6H^+ +4Na^+]^{2-}$
201	1885.989	1885.977	6.366	GD1 (d18:1/20:0)	$[M-2H^+ +Na^+]^-$
		1885.980	4.774	GD1 (d18:1/22:3)	$[M-H^+]^-$
		1886.016	14.316	*O*−Ac GT3 (d18:1/24:1)	$[M-H^+]^-$
202	1889.993	1889.949	23.292	GD1 (d18:1/20:0)	$[M-H_2O-3H^+ +2Na^+]^-$
		1890.011	9.528	GD1 (d18:1/22:1)	$[M-H^+]^-$
		1890.048	29.115	*O*−Ac GT3 (d18:0/24:0)	$[M-H^+]^-$

[a]Abbreviations and abbreviations used for gangliosides. ***Ac***: acetyl/acetylation; ***Cer***: ceramide; ***LacCer***: Galβ_4Glcβ_1Cer; ***GM3***: II^3-α-Neu5Ac-LacCer; ***GD3***: II^3-α-(Neu5Ac)$_2$-LacCer; ***GT3***: II^3-α-(Neu5Ac)$_3$-LacCer; ***GM2***: II^3-α-Neu5Ac-Gg$_3$Cer; ***GD2***: II^3-α-(Neu5Ac)$_2$-Gg$_3$Cer; ***GM1a or GM1***: II^3-α-Neu5Ac-Gg$_4$Cer; ***GM1b***: IV^3-α-Neu5Ac-Gg$_4$Cer; ***GalNAc-GM1b***: IV^3-α-Neu5Ac-Gg$_5$Cer; ***GD1a***: IV^3-α-Neu5Ac$_2$II^3-α- Neu5Ac-Gg$_4$Cer; ***GD1b***: II^3-α-(Neu5Ac)$_2$-Gg$_4$Cer; ***GT1b***: IV^3-α-Neu5Ac,II^3-α-(Neu5Ac)$_2$-Gg$_4$Cer; ***GQ1b***: IV^3-α-(Neu5Ac)$_2$,II^3-α-(Neu5Ac)$_2$-Gg$_4$Cer; ***nLM1 or 3′-nLM1***: IV^3-α-Neu5Ac-nLc$_4$Cer; ***LM1 or 3′-isoLM1***: IV^3-α-Neu5Ac-Lc$_4$Cer; ***nLD1***: disialo-nLc4Cer

In principle, IMS separation reduces the spectral congestion by separating components into mobility families. One outcome of this separation is a reduction of background chemical noise, which normally, in a single dimension MS measurement, appears as a baseline. In the present case, following ion mobility separation, the chemical noise was dispersed across a wide range of drift times and could be easily recognized as a broad, well-defined region in Figure 1. Moreover, the 2D plot of FL37 revealed not only the separation of GGs based on the charge state but also their separation based on the carbohydrate chain length and the degree of sialylation. Obviously, the optimized ionization conditions allowed the simultaneous formation of predominantly triply-, doubly-, and singly charged ions and enhanced the ionization of long chain polysialylated structures; the entire series starting from mono- up to octasialo GGs containing a high diversity of ceramide constitutions was observed.

To enhance the differentiation of the detected ions, the proposed structures together with the corresponding *m/z* values are listed in Table 1. A remarkably rich molecular ion pattern, proving the presence of a large number of glycoforms and an unpredicted diversity of the ceramide chains for certain species, was observed. No less than 143 distinct gangliosides were identified in the FL37 sample mixture by IMS MS for the first time. This number represents more than three times the number of ganglioside species detected in similar samples from the fetal frontal lobe (i.e., FL36[26] or FL27[36]) by other MS methods, such as the fully automated chip-based nanoESI HCT MS, without previous separation.

From the total number of 143 species, 47 structures were identified as GT forms bearing ceramides of variable constitution, 37 structures as GD forms, 25 structures as GM forms, and no less than 12 structures as GQ forms. As mentioned above, according to mass calculation and based on the excellent value of the mass accuracy, several structures have been identified as bearing up to eight Neu5Ac residues. Thus, two species were identified as pentasialogangliosides (GP), while a number of five, eight, and seven species, respectively, were detected as hexasialogangliosides (GH), heptasialogangliosides (GS), and

DOI: 10.1021/acs.analchem.6b00155
Anal. Chem. 2016, 88, 5166−5178

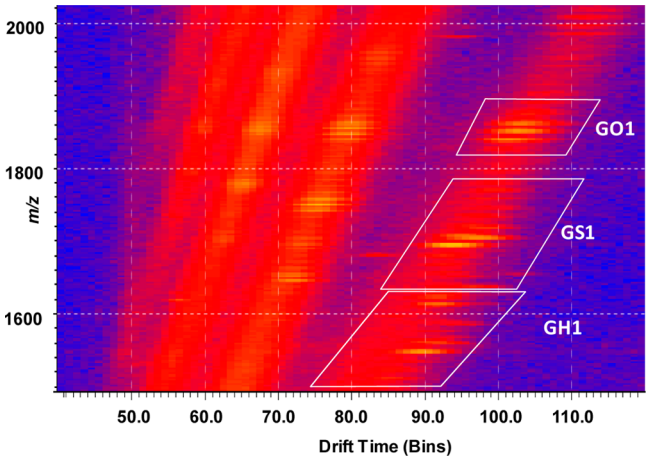

Figure 2. Expansion of driftscope display for m/z area between 1500 and 2100 outlines the separation of the three doubly charged ganglioside classes: between 1500 and 1624 m/z were identified as GH1 species; between 1675 and 1791 m/z were identified as GS1 species; and between 1834 and 1887 m/z were identified as GO1 species. The extracted spectra for all three ganglioside classes are presented in Figure 4b.

octasialogangliosides (GO) (Figure 1 and Figure 2). Up to now, pentasialylated species represented the highest polysialylated gangliosides detected in human brain by MS.[42] The identification in the FL37 mixture of gangliosides with a much higher degree of sialylation was possible only due to the ion mobility separation that allowed the differentiation of GGs based on carbohydrate chain length and the degree of sialylation. By integrating the data over narrow regions where the signals afferent to polysialylated species appear, it was possible to reduce contributions due to the background noise and identify low-abundance species present in the brain, which were not detectable before using other MS methods. The incidence of polysialylation in FL37 is in agreement with the previous studies that demonstrated the existence of a direct correlation between ganglioside sialylation and brain developmental stage.[14,27,36,41,49] A high sialylation is characteristic for fetal brains: the sialylation degree is increased in the incipient intrauterine developmental stages and decreases during fetus development. Since the 37th gw corresponds to the last pregnancy trimester, an advanced level of intrauterine development, the number of highly sialylated GG species follows the descending series GT > GQ > GS > GO > GH > GP. Consequently, these findings based on IMS MS provide a more reliable insight into the expression of polysialylated structures, which might constitute markers of brain development and/or brain diseases.

The presence of biologically relevant species modified by peripheral attachments such as *O*-fucosylation and *O*-acetylation was previously reported as being associated with the tissue in its advanced developmental phase.[50,51] The data generated by IMS MS for the FL37 sample support this concept because no less than 17 fucosylated species, of which two GM1, four GD1, four GT1, and seven GT3 as well as 18 *O*-acetylated structures corresponding to GM1, GD1, GD3, GT1, GT3, and GQ1, exhibiting high heterogeneity in their ceramide motifs, were discovered.

Most of the structures identified in FL37 sample, more precisely a number of 101, exhibited dihydroxylated sphingoid bases, while only 42 gangliosides having trihydroxylated sphingoid bases were found. The incidence in human tissues of ganglioside species exhibiting trihydroxylated sphingoid bases (t18:0) and (t18:1) was reported previously in epithelial cells of the small intestine,[52] fetal hippocampus,[35] fetal frontal lobe,[34,36] fetal neocortex,[42] as well as in adult human cerebellum[43] and adult sensory and motor cortex.[53] Obviously, trihydroxylation of the sphingoid base is a process accompanying the human brain along the intrauterine and extrauterine development.

By extracting and retaining the drift time for each narrow region indicated in Figure 1 and by combining the extracted ion chromatograms (XICs), the corresponding spectrum for each GG class was generated. It was not possible in only a few cases to allocate a well-defined area for a specific GG group due to the mass intercalation of two different GG groups, one with a shorter carbohydrate chain and a longer ceramide composition and another one with longer carbohydrate chain and a shorter ceramide composition (i.e., GM1 overlapped with GD3, while GD1 overlapped with GT3). A clear example is illustrated in Figure 3, where between 1300 and 1720 m/z range several singly charged species belonging to GM1 and GD3 groups could be found.

No less than five spectra corresponding to GM3, GM2, GM1 together with GD3, GD2, and GD1 (Figure 4a), respectively, were generated from the XIC of the singly charged species. At the same time, the doubly charged structures listed in Table 1 originate from Figure 4b, in which are presented no less than eight spectra arising from GD3, GD2, GD1 together with GT3, GT1, GQ1, GH1, GS1 and GO1 gangliosides. Following the same procedure, after extracting and combining XIC for the triply charged species

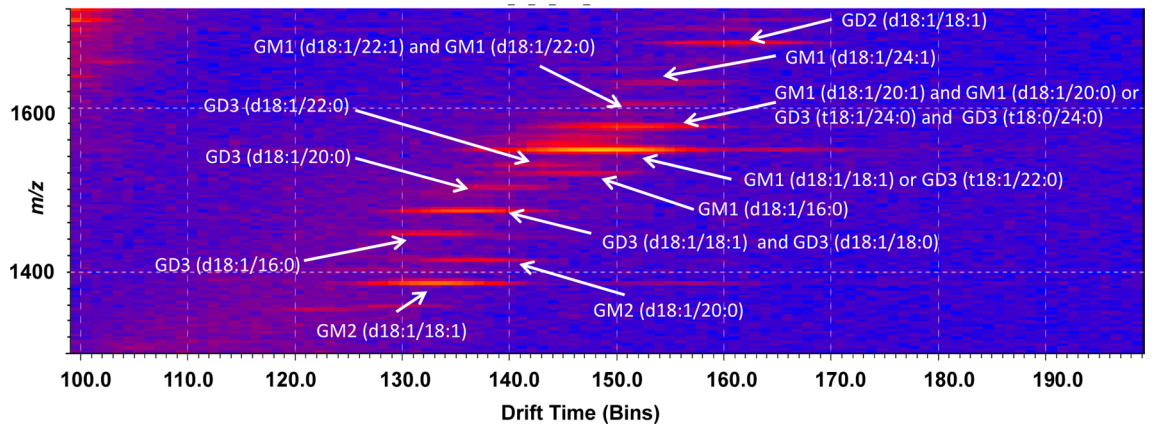

Figure 3. Expansion of driftscope display for m/z area between 1300 and 1720 clearly showing the separation based on the carbohydrate chain length of the singly charged gangliosides.

DOI: 10.1021/acs.analchem.6b00155
Anal. Chem. 2016, 88, 5166−5178

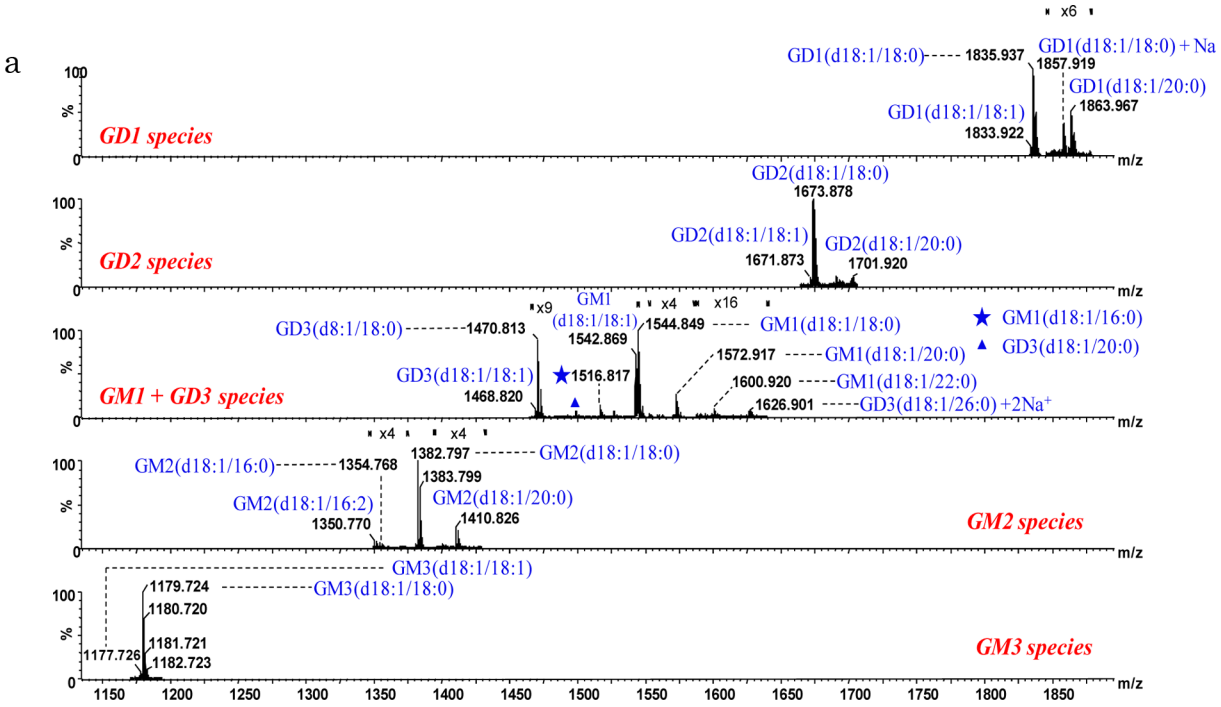

Figure 4a. Extracted mass spectra of singly charged GM3, GM2, GM1 together with GD3, GD2, and GD1 gangliosides from the corresponding areas indicated in Figure 1.

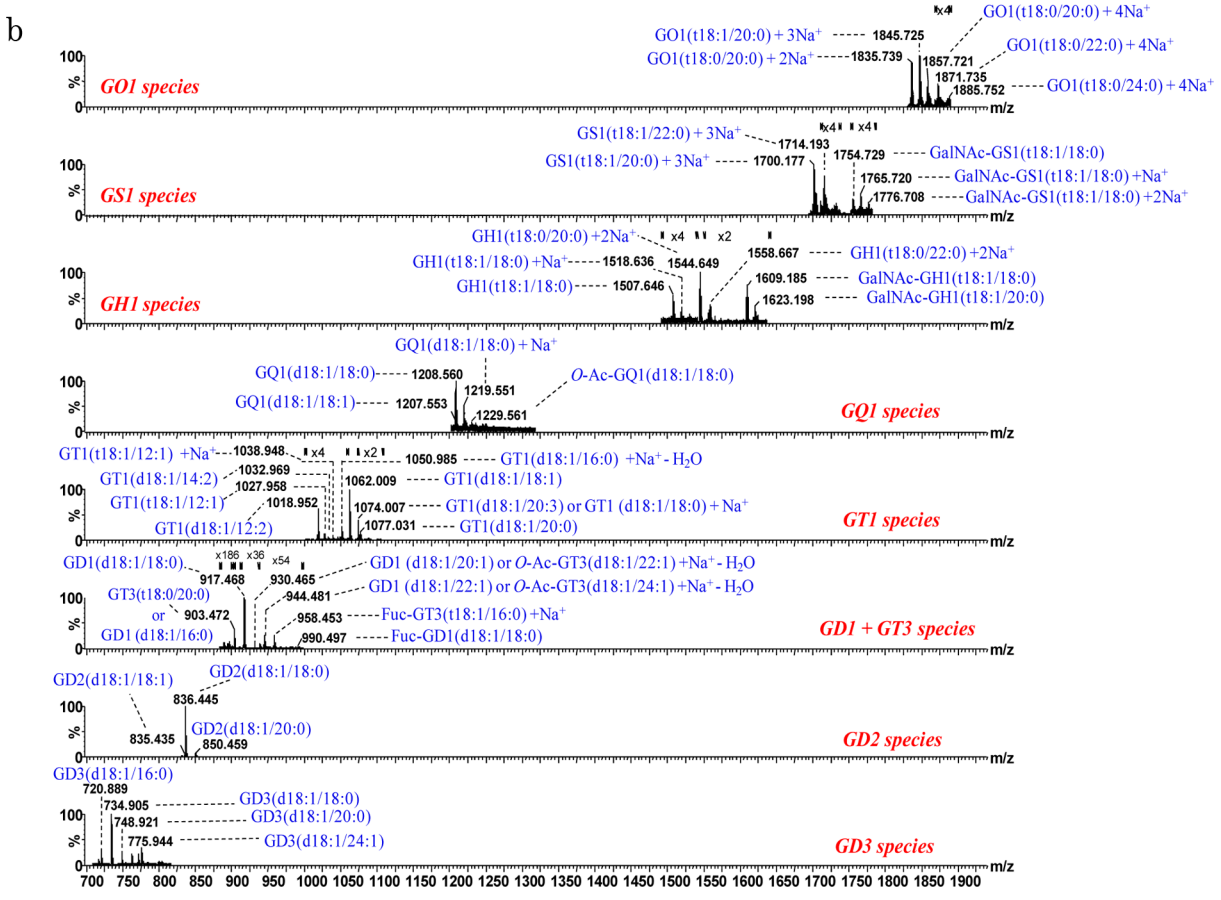

Figure 4b. Extracted mass spectra of doubly charged GD3, GD2, GD1 together with GT3, GT1, GQ1, GH1, GS1 and GO1 gangliosides from the corresponding areas indicated in Figure 1.

indicated in Figure 1, seven spectra were generated, of which the five spectra related to GGs exhibiting the highest diversity of ceramides are presented in Figure 4c. These correspond to GD1 together with GT3, GT1, GQ1, GS1, and GO1 classes.

DOI: 10.1021/acs.analchem.6b00155
Anal. Chem. 2016, 88, 5166−5178

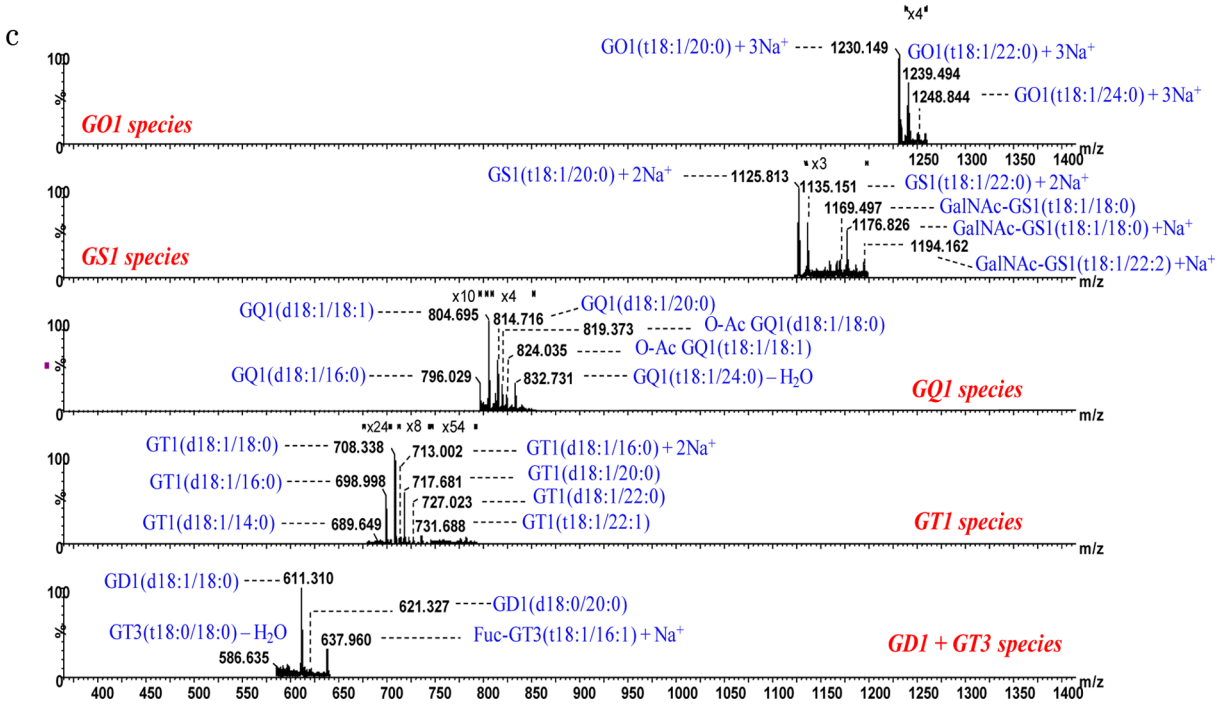

Figure 4c. Extracted mass spectra of triply charged GD1 together with GT3, GT1, GQ1, GS1 and GO1 gangliosides from the corresponding areas indicated in Figure 1.

Fragmentation Analysis of GalNAc–GQ1 by IMS CID MS/MS. To test for the first time the feasibility of IMS CID MS/MS in structural analysis of gangliosides, a number of molecular ions, which according to mass calculation correspond to structures known as associated with fetal brain, were submitted to fragmentation analysis. MS/MS data confirmed the structure of previously characterized[34,36,42,43] GM1(d18:1/18:0), GM2(d18:1/20:0), GM3(d18:1/18:0), GD1(d18:1/18:0), and GT1(d18:1/18:0) species, detected here as mono- to triply deprotonated molecules at m/z 1544.849, 1410.826, 1179.724, 1835.937, and 708.338, respectively. However, by IMS CID MS/MS, structural data on a novel species could be collected as well. For instance, in Figure 5, the fragmentation analysis of the $[M-3H^+ + Na^+]^{2-}$ at m/z 1321.121, which according to mass calculation corresponds to GalNAc–GQ1 (d18:1/18:0) is presented. We have chosen to present this particular ion for the following reasons: (i) this novel structure is of high sialylation degree and hence among the species with potential marker role in fetal brain; (ii) according to mass calculation the species belongs to the G1 class characterized by the longest carbohydrate chain, which is supplementary extended by an *O*-linked GalNAc residue, a relatively rare modification for gangliosides.

The ion was isolated by setting LM to 10 and HM to 15 and further submitted to CID MS/MS under variable collision energy within 10–45 eV. The tandem mass spectrum is depicted in Figure 5, while the scheme illustrating the fragmentation pathway experienced by this ion under the employed conditions is shown in Figure 6. The high number of sequence ions observed in the spectrum in Figure 5, diagnostic for the proposed structure, reveals that the conditions for ionization and fragmentation were properly optimized in order to generate high sequence coverage for this type of substrates.

The tetrasialylation of this species is documented by $B_{4\beta}^-$ fragment ion at m/z 1163.436, $C_{4\beta}^-$ at m/z 1181.444, together with the sodiated $[B_{4\beta}-2H^+ + Na^+]^-$ form at m/z 1185.486 and the doubly sodiated dehydrated $[C_{4\beta}-H_2O-3H^+ + 2Na^+]^-$ at m/z 1207.338, corresponding to the tetrasialo element $(Neu5Ac)_4$. The tetrasialo element is actually supported by the presence of the entire $B_{1\beta}-B_{4\beta}$ series of fragment ions, together with $C_{1\beta}-C_{4\beta}$ series, as depicted in Figure 5. These ions demonstrate that all four Neu5Ac residues are linked together in the ganglioside structure.

Furthermore, the doubly charged fragment ion $[B_4-2H^+]^{2-}$ at m/z 946.391 together with the doubly charged fragment ion $[C_4-2H^+]^{2-}$ at m/z 955.396, $[B_5-2H_2O-3H^+ + Na^+]^{2-}$ at m/z 1020.498 and $[C_5-H_2O-2H^+]^{2-}$ at m/z 1018.332, corroborate the attachment of the tetrasialo element to the inner Gal of the oligosaccharide backbone. This structural concept is further supported by the following fragment ions: $[Z_{2\alpha}-2H_2O-2H^+]^{2-}$ at m/z 999.003, $[Z_{2\alpha}-H_2O-2H^+]^{2-}$ at m/z 1001.086, $[Y_{2\alpha}-2H_2O-3H^+ + Na^+]^{2-}$ at m/z 1019.067, $[Z_{3\alpha}-H_2O-2H^+]^{2-}$ at m/z 1100.416, $[Z_{4\alpha}-3H^+ + Na^+]^{2-}$ at m/z 1210.576 and $[Y_{4\alpha}-2H^+]^{2-}$ at m/z 1208.664. All these ions allow to conclude that $(Neu5Ac)_4$ is attached to the inner Gal, which indicates that the fragmented ganglioside species belongs to the *d* series.

Other fragment ions such as $[Y_{5\beta}-3H^+ + Na^+]^{2-}$ at m/z 1175.573, $[Z_{4\beta}-2H_2O-2H^+]^{2-}$ at m/z at 992.098, $[Y_{3\beta}-3H^+ + 2Na^+]^-$ at m/z 1791.901 and $[Y_{2\beta}-3H^+ + 2Na^+]^-$ at m/z 1500.863 further support the structure proposed in Figure 6. Also, besides the frequently observed cleavage of one glycosidic bond, a number of double or triple bond cleavages of high structural relevance were induced under the optimized sequencing conditions. $Y_{2\alpha}/B_{4\beta}^-$ fragment ion at m/z 888.785 corresponds to Gal–Glc–Cer, which represents the reducing end of the ganglioside species with (d18:1/18:0) ceramide moiety. Additionally, the following fragment ions substantiate GalNAc–GQ1 (d18:1/18:0) structure: $Y_{4\alpha}/B_{3\beta}^-$ at m/z 1544.963, together with its doubly sodiated dehydrated form $[Y_{4\alpha}/B_{3\beta}-H_2O-3H^+ + 2Na^+]^-$ at m/z 1570.714 and its sodiated doubly charged form $[Y_{4\alpha}/B_{3\beta}-3H^+ + Na^+]^{2-}$ at m/z 780.091,

DOI: 10.1021/acs.analchem.6b00155
Anal. Chem. 2016, 88, 5166–5178

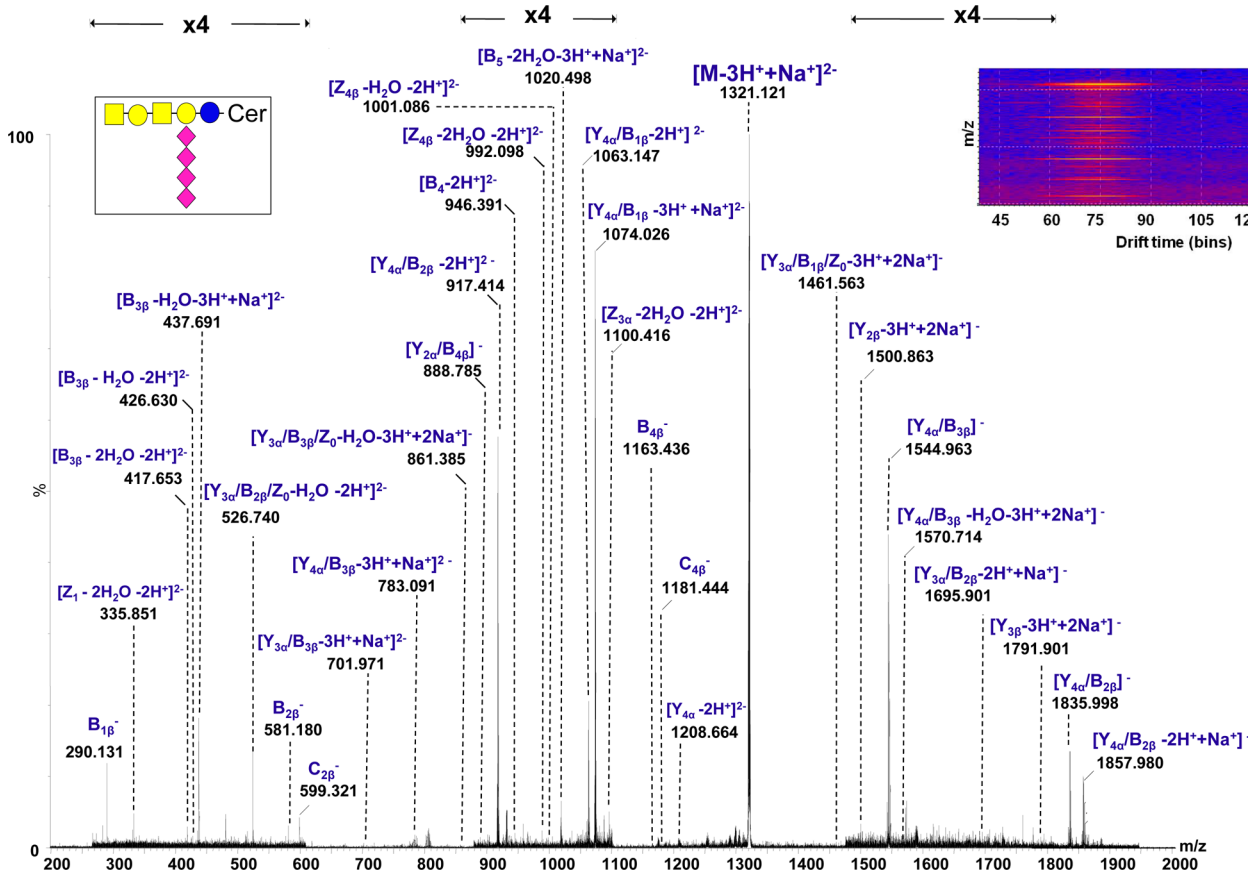

Figure 5. (−) ESI IMS CID MS/MS of the $[M+Na^+-3H^+]^{2-}$ at m/z 1321.121 corresponding to GalNAc−GQ1d (d18:1/18:0) species fragmented from FL37 sample. Inset left: the structure of the precursor ion. Inset right: driftscope display of the IMS CID MS/MS product ions. Cone voltage 40 V. Capillary voltage 2 kV. Acquisition 300 scans. CID at variable collision energy within 10−45 eV. yellow ■ − GalNAc; yellow ● − Gal; blue ● − Glc; pink ◆ − Neu5Ac.

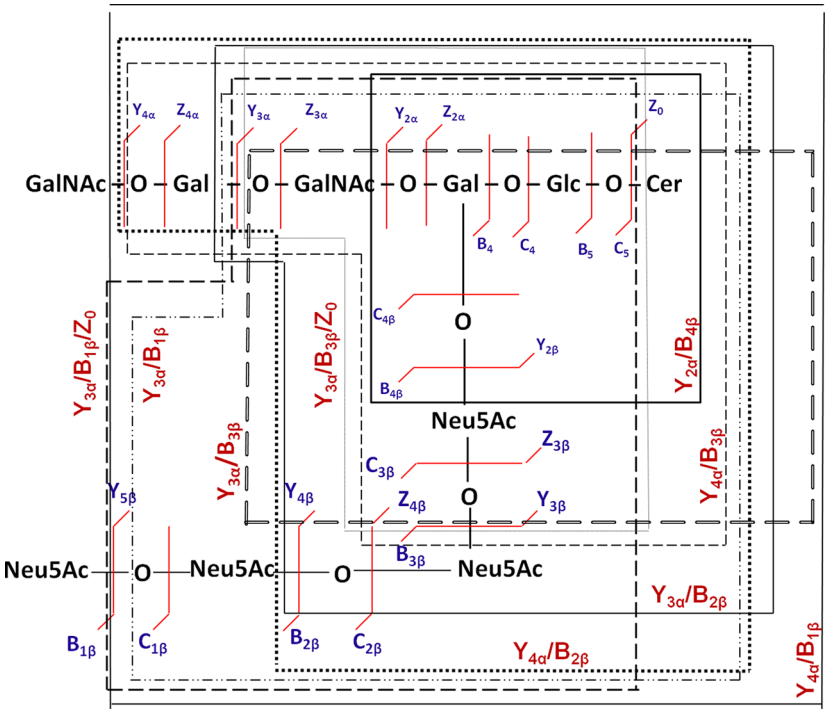

Figure 6. Fragmentation scheme by IMS CID MS/MS of GalNAc−GQ1d species.

DOI: 10.1021/acs.analchem.6b00155
Anal. Chem. 2016, 88, 5166−5178

$Y_{4\alpha}/B_{2\beta}^{-}$ at m/z 1835.998, together with its sodiated form $[Y_{4\alpha}/B_{2\beta}-2H^{+}+Na^{+}]^{-}$ at m/z 1857.980 and its doubly charged form $[Y_{4\alpha}/B_{2\beta}-2H^{+}]^{2-}$ at m/z 917.414.

$[Y_{4\alpha}/B_{1\beta}-2H^{+}]^{2-}$ at m/z 1063.147, along with $[Y_{3\alpha}/B_{1\beta}-2H^{+}]^{2-}$ at m/z 982.016, $[Y_{3\alpha}/B_{2\beta}-2H^{+}+Na^{+}]^{-}$ at m/z 1695.901 and $[Y_{3\alpha}/B_{3\beta}-3H^{+}+Na^{+}]^{2-}$ at m/z 701.971 as well as the triple bond cleavage fragment ions $[Y_{3\alpha}/B_{1\beta}/Z_0-3H^{+}+2Na^{+}]^{-}$ at m/z 1461.563, $[Y_{3\alpha}/B_{3\beta}/Z_0-H_2O-3H^{+}+2Na^{+}]^{-}$ at m/z 861.385 confirm the proposed structure.

CONCLUSIONS

In the present study, IMS MS was for the first time introduced in glycolipidomics of the human brain. The method was explored and developed for the characterization of a highly complex native ganglioside mixture extracted and purified from a normal fetal frontal lobe in the 37th gestational week. The results obtained here indicate that IMS MS is a powerful and highly efficient technique able to unequivocally detect and characterize glycolipid species with potential biomarker role. By this approach, the two-dimensional data set of FL37, generated after 6 min of signal acquisition, revealed a large number of glycoforms and an elevated diversity of the ceramide chain for certain species. By combining direct ionization with IMS and high-resolution MS, a total number of 143 distinct gangliosides exhibiting a high degree of heterogeneity, were identified and assigned with an average mass accuracy of 11.402 ppm.

In the previous studies related to highly complex mixtures of gangliosides extracted and purified from various human brain regions performed on HCT, FTICR, and/or QTOF MS without any separation prior to mass analysis, the maximum degree of sialylation was found to be five. Here, the identification in human brain for the first time of GG species presenting a much higher sialylation degree ranging from mono- up to octasialogangliosides could be achieved based on IMS MS capability to (i) diminish the spectral congestion by separating components into mobility families; (ii) reduce the background chemical noise concomitantly with increasing the signal-to-noise ratio; (iii) rapid separate the ions based on size/charge ratio; (iv) differentiate the gangliosides, based on the carbohydrate chain length and the degree of sialylation; (v) extract ion chromatograms for narrow regions in order to detect species that are low expressed in brain tissue. The existence of a direct correlation between ganglioside sialylation degree and brain developmental stage, where higher sialylation levels are characteristic for incipient intrauterine developmental phases was fully confirmed by the obtained results.

The structural confirmation of a new and biologically relevant species modified by GalNAc attachment was achieved by CID MS/MS under variable collision energy after mobility separation in the transfer cell. The optimized isolation and fragmentation conditions induced efficient ion dissociation with high sequence coverage and ions diagnostic for the proposed structures of the sugar core and ceramide moiety. No less than 40 diagnostic fragment ions for GalNAc−GQ1 (d18:1/18:0) were generated; of these, 10 provide hard evidence on the existence of the tetrasialo element attached to the inner Gal, indicating that the fragmented ganglioside species belongs to the *d* series.

Consequently, in the present study, IMS MS and IMS CID MS/MS were successfully implemented in human brain ganglioside research. These initial findings provide a solid platform for further development of IMS MS-based methodologies, which represent promising novel tools for the characterization of gangliosides extracted as native mixtures from human matrices.

AUTHOR INFORMATION

Corresponding Author

*E−mail: alinazamfir@yahoo.com. Tel./Fax: +40−256−494413.

Notes

The authors declare no competing financial interest.

ACKNOWLEDGMENTS

This work was supported by the Romanian National Authority for Scientific Research, UEFISCDI, projects PN-II-ID-PCE-2011-3-0047, PN-II-PCCA-2011-142, PN-II-PCCA-2013-4-0191 granted to A.D.Z.

REFERENCES

(1) Kanu, A. B.; Dwivedi, P.; Tam, M.; Matz, L.; Hill, H. H., Jr. *J. Mass Spectrom.* **2008**, *43*, 1−22.
(2) Shvartsburg, A. A.; Isaac, G.; Leveque, N.; Smith, R. D.; Metz, T. O. *J. Am. Soc. Mass Spectrom.* **2011**, *22*, 1146−1155.
(3) Eiceman, G. A.; Karpas, Z. *Ion Mobility Spectrometry*, 2nd ed.; CRC Press: Boca Raton, FL, 2005.
(4) Shvartsburg, A. A. *Differential ion mobility spectrometry*; CRC Press: Boca Raton, FL, 2008.
(5) Hofmann, J.; Struwe, W. B.; Scarff, C. A.; Scrivens, J. H.; Harvey, D. J.; Pagel, K. *Anal. Chem.* **2014**, *86*, 10789−10795.
(6) Paglia, G.; Angel, P.; Williams, J. P.; Richardson, K.; Olivos, H. J.; Thompson, J. W.; Menikarachchi, L.; Lai, S.; Walsh, C.; Moseley, A.; Plumb, R. S.; Grant, D. F.; Palsson, B. O.; Langridge, J.; Geromanos, S.; Astarita, G. *Anal. Chem.* **2015**, *87*, 1137−1144.
(7) Uetrecht, C.; Rose, R. J.; van Duijn, E.; Lorenzen, K.; Heck, A. *Chem. Soc. Rev.* **2010**, *39*, 1633−1655.
(8) Fenn, L. S.; Kliman, M.; Mahsut, A.; Zhao, S. R.; McLean, J. A. *Anal. Bioanal. Chem.* **2009**, *394*, 235−244.
(9) Merenbloom, S. I.; Koeniger, S. L.; Valentine, S. J.; Plasencia, M. D.; Clemmer, D. E. *Anal. Chem.* **2006**, *78*, 2802−2809.
(10) Bush, M. F.; Campuzano, I. D. G.; Robinson, C. V. *Anal. Chem.* **2012**, *84*, 7124−7130.
(11) Niu, S.; Rabuck, J. N.; Ruotolo, B. T. *Curr. Opin. Chem. Biol.* **2013**, *17*, 809−817.
(12) Kliman, M.; May, J. C.; McLean, J. A. *Biochim. Biophys. Acta, Mol. Cell Biol. Lipids* **2011**, *1811*, 935−945.
(13) Kyle, J. E.; Zhang, X.; Weitz, K. K.; Monroe, M. E.; Ibrahim, Y. M.; Moore, R. J.; Cha, J.; Sun, X.; Lovelace, E. S.; Wagoner, J.; Polyak, S. J.; Metz, T. O.; Dey, S. K.; Smith, R. D.; Burnum−Johnson, K. E.; Baker, E. S. *Analyst* **2016**, *141*, 1649−1659.
(14) Milic, I.; Kipping, M.; Hoffmann, R.; Fedorova, M. *J. Mass Spectrom.* **2015**, *50*, 1386−1392.
(15) Groessl, M.; Graf, S.; Knochenmuss, R. *Analyst* **2015**, *140*, 6904−6911.
(16) Pagel, K.; Harvey, D. J. *Anal. Chem.* **2013**, *85*, 5138−5145.
(17) Hofmann, J.; Hahm, H. S.; Seeberger, P. H.; Pagel, K. *Nature* **2015**, *526*, 241−244.
(18) Gaye, M. M.; Kurulugama, R.; Clemmer, D. E. *Analyst* **2015**, *140*, 6922−6932.
(19) Leary, J. A.; Miller, R. L.; Wei, W.; Schwörer, R.; Zubkova, O. V.; Tyler, P. C.; Turnbull, J. E. *Eur. Mass Spectrom.* **2015**, *21*, 245−254.
(20) Lapthorn, C.; Pullen, F.; Chowdhry, B. Z. *Mass Spectrom. Rev.* **2013**, *32*, 43−71.
(21) Wiegandt, H., In: *Structure and Function of Gangliosides*; Svennerholm, L., Ed.; Springer Science & Business Media: New York, 2012; pp 3−10.
(22) Vukelić, Ž.; Metelmann, W.; Müthing, J.; Kos, M.; Peter-Katalinic, J. *Biol. Chem.* **2001**, *382*, 259−274.
(23) Schnaar, R. L.; Gerardy−Schahn, R.; Hildebrandt, H. *Physiol. Rev.* **2014**, *94*, 461−518.
(24) Posse de Chaves, E.; Sipione, S. *FEBS Lett.* **2010**, *584*, 1748−1759.
(25) Ono, M.; Hakomori, S. *Glycoconjugate J.* **2003**, *20*, 71−78.
(26) Kaida, K.; Ariga, T.; Yu, R. K. *Glycobiology* **2009**, *19*, 676−692.

DOI: 10.1021/acs.analchem.6b00155
Anal. Chem. 2016, 88, 5166−5178

(27) Yuki, N. *Proc. Jpn. Acad., Ser. B* **2012**, *88*, 299−326.
(28) Bisel, B.; Pavone, F. S.; Calamai, M. *Biomol. Concepts* **2014**, *5*, 87−93.
(29) Utz, J. R.; Crutcher, T.; Schneider, J.; Sorgen, P.; Whitley, C. B. *Mol. Genet. Metab.* **2015**, *114*, 274−280.
(30) Morgado, I.; Garvey, M. *Adv. Exp. Med. Biol.* **2015**, *855*, 67−94.
(31) Müthing, J. *Methods Enzymol.* **2000**, *312*, 45−64.
(32) Müthing, J. *Methods Mol. Biol.* **1998**, *76*, 183−195.
(33) Mosoarca, C.; Ghiulai, R. M.; Novaconi, C. R.; Vukelić, Z.; Chiriac, A.; Zamfir, A. D. *Anal. Lett.* **2011**, *44*, 1036−1049.
(34) Serb, A.; Schiopu, C.; Flangea, C.; Vukelić, Ž.; Sisu, E.; Zagrean, L.; Zamfir, A. D. *Eur. Mass Spectrom.* **2009**, *15*, 541−553.
(35) Vukelić, Ž.; Zarei, M.; Peter−Katalinic, J.; Zamfir, A. D. *J. Chromatogr. A* **2006**, *1130*, 238−245.
(36) Almeida, R.; Mosoarca, C.; Chirita, M.; Udrescu, V.; Dinca, N.; Vukelić, Ž.; Allen, M.; Zamfir, A. D. *Anal. Biochem.* **2008**, *378*, 43−52.
(37) Vukelić, Ž.; Kalanj-Bognar, S.; Froesch, M.; Bindila, L.; Radic, B.; Allen, M.; Peter-Katalinić, J.; Zamfir, A. D. *Glycobiology* **2007**, *17*, 504−515.
(38) Schiopu, C.; Vukelić, Ž.; Capitan, F.; Kalanj−Bognar, S.; Sisu, E.; Zamfir, A. D. *Electrophoresis* **2012**, *33*, 1778−1786.
(39) Schiopu, C.; Flangea, C.; Capitan, F.; Serb, A.; Vukelić, Ž.; Kalanj−Bognar, S.; Sisu, E.; Przybylski, M.; Zamfir, A. D. *Anal. Bioanal. Chem.* **2009**, *395*, 2465−2477.
(40) Jackson, S. N.; Colsch, B.; Egan, T.; Lewis, E. K.; Schultz, J. A.; Woods, A. S. *Analyst* **2011**, *136*, 463−466.
(41) Saito, M.; Sugiyama, K. *Biochim. Biophys. Acta, Gen. Subj.* **2000**, *1474*, 88−92.
(42) Ghiulai, R. M.; Sarbu, M.; Vukelić, Ž.; Ilie, C.; Zamfir, A. D. *Glycoconjugate J.* **2014**, *31*, 231−245.
(43) Zamfir, A.; Vukelić, Z.; Bindila, L.; Peter−Katalinić, J.; Almeida, R.; Sterling, A.; Allen, M. *J. Am. Soc. Mass Spectrom.* **2004**, *15*, 1649−1657.
(44) Serb, A. F.; Sisu, E.; Vukelić, Ž.; Zamfir, A. D. *J. Mass Spectrom.* **2012**, *47*, 1561−1570.
(45) Svennerholm, L.; Fredman, P. *Biochim. Biophys. Acta, Lipids Lipid Metab.* **1980**, *617*, 97−109.
(46) Svennerholm, L. *Adv. Exp. Med. Biol.* **1980**, *125*, 11.
(47) IUPAC−IUB Joint Commission on Biochemical Nomenclature. *Eur. J. Biochem.* **1998**, *257*, 293−298.
(48) Domon, B.; Costello, C. E. *Glycoconjugate J.* **1988**, *5*, 397−409.
(49) Svennerholm, L. *Adv. Genet.* **2001**, *44*, 33−41.
(50) Costello, C. E.; Juhasz, P.; Perreault, H. *Prog. Brain Res.* **1994**, *101*, 45−61.
(51) Kusunoki, S.; Inoue, K.; Iwamori, M.; Nagai, Y.; Mannen, T.; Kanazawa, I. *Neurosci. Res.* **1992**, *15*, 74−80.
(52) Breimer, M. E.; Hansson, G. C.; Karlsson, K. A.; Larson, G.; Leffler, H. *Glycobiology* **2012**, *22*, 1721−1730.
(53) Flangea, C.; Fabris, C.; Vukelić, Ž.; Zamfir, A. D. *Aust. J. Chem.* **2013**, *66*, 781−790.

DOI: 10.1021/acs.analchem.6b00155
Anal. Chem. 2016, 88, 5166−5178